New Fault-Resistance Estimation Algorithm for Rotor-Winding Ground-Fault Online Location in Synchronous Machines With Static Excitation

Francisco R. Blánquez, Francisco Blázquez, María Aranda, Emilio Rebollo, and Carlos A. Platero

***Abstract*—This paper presents a new algorithm for estimating the ground-fault resistance value in rotor windings. This new algorithm is an improvement of an online ground-fault location method previously presented. This location method is suitable for synchronous generators with static excitation, whose excitation field winding is fed by controlled rectifiers through an excitation transformer. The estimation of the fault resistance is obtained through the comparison between the third-harmonic voltage measured in a grounding resistance placed in the neutral of the excitation transformer and the third-harmonic voltage calculated by the algorithm. This latter variable is obtained with the dc component of the output voltage of the controlled rectifier and the ac supply voltage of this converter. The fault resistance value is used in the novel technique of online ground-fault location, and it allows improving the accuracy of the location of the defect. This new algorithm, integrated in the complete location method, has been tested with satisfactory results in a 5-kVA laboratory synchronous generator and in a 106-MVA hydrogenerating unit.**

***Index Terms*—Alternators, fault detection, fault diagnosis, fault location, generators, protection, rotating machines, rotors.**

Nomenclature

f_1	Network frequency.
N	Neutral point.
R_G	Grounding resistance.
R_F	Fault resistance.
R_F^*	Estimation of fault resistance.
x	Location of the ground fault, from 0% (negative terminal) to 100% (positive terminal).
x^*	Estimation of ground-fault location, from 0% (negative terminal) to 100% (positive terminal).
α	Firing angle of the controlled rectifier.
α^*	Estimation of the firing angle of the controlled rectifier.
V	Voltage measurement in the grounding resistance.
V_f	Voltage measurement in the field winding.
V_{ph}	Voltage measurement in the low-voltage side of the excitation transformer.
$V_{AC,f}$	AC component at f_1 of the grounding-resistance voltage measurement.
$V_{AC,3f}$	AC component at $3 \cdot f_1$ of the grounding-resistance voltage measurement.
$V^*_{AC,3fM}$	Estimation of the maximum value of $V_{AC,3f}$.
V_{DC}	DC component of the grounding-resistance voltage measurement.
V_{DC0}	Maximum value of V_{DC}.
$V_{fAC,6f}$	AC component at $6 \cdot f_1$ of the field-winding voltage measurement.
V_{fDC}	DC component of the field-winding voltage measurement.
$V_{phAC,f}$	AC component at f_1 of the excitation-transformer voltage measurement.
$thrf$	Setting threshold for the f_1 comparison in the ac–dc discrimination block.
$thr3f$	Setting threshold for the $3 \cdot f_1$ comparison in the ac–dc discrimination block.
V_{AN}	Phase-to-neutral voltages in the excitation transformer (phase A).
V_{AB}	Phase-to-phase voltages in the excitation transformer (phase A–phase B).
A_1, B_1	Frequency-component coefficients at $3 \cdot f_1$ for the calculation of $V^*_{AC,3fM}$.
E	Error in the fault location by the new method.
x_p^*	Fault location obtained by the previous method.
E_p	Error in the fault location by the previous method.

The authors are with the Electrical Engineering Department of the ETSII (Polytechnic University of Madrid), 28006 Madrid, Spain (e-mail: fr.blanquez@gmail.com).

I. Introduction

ELECTRICAL protections are absolutely vital to safeguard the power systems against short circuits, abnormal operating conditions, overloads, and, in general, any type of events that threaten the reliability of the network. In power plants, the generating unit is the most important element. Therefore, protective systems focus specially on protecting generators [1]. In synchronous generators, the most common malfunctions, such as unbalanced stator voltages or vibrations, are caused by ground faults in the rotor winding. The excitation field circuit of synchronous generators is typically isolated during normal operating conditions. The field winding is exposed to mechanical and thermal stress cycles due to the rotation speed and the temperature increase [2]. In addition to the normal stress, the field winding can be exposed to abnormal

mechanical or thermal stress due to overspeed, vibrations [3], excessive field currents, poor cooling or stator negative sequence currents, among some others. This may result in a breakdown of the insulation between the field winding and the rotor iron at the points where the stress has the highest values. As the excitation system is isolated, a single ground fault in the field winding, or its associated circuits, causes a negligible fault current, which does not represent any immediate danger. However, if a second ground fault occurs, high fault currents and severe mechanical unbalances may quickly arise, leading to serious damage. In some cases, the field current, flowing through the rotor iron, could generate enough heat to melt it [4], [5]. It is essential, therefore, that the first insulation failure has to be detected [6]–[8], and the generator has to be removed from service to check the insulation health [9].

Most rotor ground-fault detection devices used for synchronous generators are based on the detection of abnormal values in certain electrical variables, such as the stator no-load voltage [10], or the air gap flux [11]; thus, they can only detect double faults. Some other commercial detection devices precise an external injection voltage source, and they are based on the detection of the current that the source provides in case of ground fault. For synchronous generators with static excitation, a novel ground-fault detection algorithm has been presented, which not only detects the defect without any additional voltage source but also discriminates between a ground fault in the ac or the dc side of the excitation system [12]. This technique requires a high-value grounding resistance to be connected to the neutral point of the excitation transformer.

On the other hand, the ground-fault location can be a costly and laborious process, particularly in multipole synchronous generators. With the exception of some cases [13], the location of the field-winding ground faults requires for the generator to be removed from service and the rotor to be extracted. The rotor diagnosis has been extensively studied in induction machines [14]–[22], where many significant contributions that have been recently presented related to interturn fault detection [23]–[26], broken-bar detection [27]–[30], and asymmetries detection [31]–[33]. However, for synchronous machines, although important studies related to permanent-magnet synchronous machines [34]–[36] or rotor eccentricity [37], [38] have been recently published, in the topic of fault detection and location in the field winding, there are not many contributions [39]–[42]. Concretely, the rotor ground-fault location is performed in a standstill condition, requiring a high-power external power source and a voltmeter, which sometimes has to have sensibility of millivolts [43].

A novel location algorithm has been previously presented [44], which implies two major advantages. First, it does not need an additional voltage source. Second, this new technique locates the defect in online operation.

This novel location algorithm requires the estimation of the fault resistance value to obtain the position of the defect. The value of the fault resistance is obtained through the voltage measurements in the grounding resistance and in the output of the controlled rectifier of the excitation system. However, the accuracy of this estimation has an influence on the precision of the fault location.

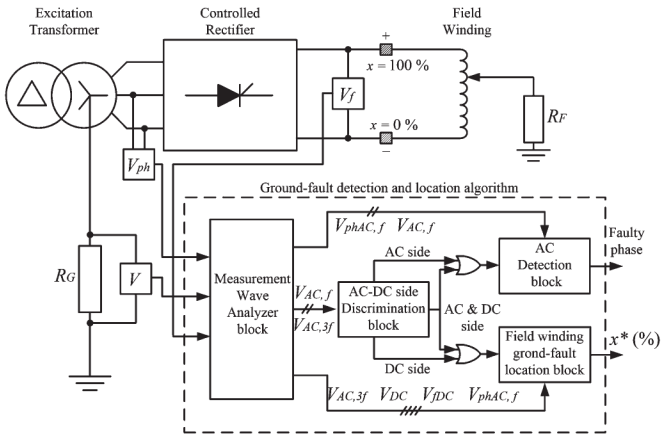

Fig. 1. Rotor ground-fault location method layout.

This paper presents a novel algorithm for the estimation of the fault-resistance value. It is based on the comparison between the third-harmonic component of the voltage in the grounding resistance and the third-harmonic voltage expected. This latter voltage is obtained by measuring the dc output voltage of the controlled rectifier and the ac supply voltage of this power converter. This new algorithm of fault-resistance value estimation, integrated in the location method previously presented [44], has been tested with satisfactory results in a 5-kVA laboratory synchronous generator and a 106-MVA commercial generating unit.

This paper first presents a brief description of the complete rotor ground-fault location method. The novel fault-resistance value estimation algorithm is described in Section III. The results of the test in the laboratory machine and in the commercial generator are described in Sections IV and V, respectively. Section VI concludes the main contribution of this research.

II. Brief Description of the Rotor Ground-Fault Location Method

This method first allows for the discrimination as to whether the ground fault is on the ac side or on the dc side of the excitation system. In addition, if the fault is located on the dc side, it is possible to provide an estimation of the ground-fault location along the field winding. If the fault is on the ac side, the algorithm detects the faulty phase and obtains the fault resistance. As additional equipment, a high-value grounding resistance is required at the excitation transformer low-voltage side. The grounding-resistance value (R_G) should be calculated to limit the ground-fault current to an acceptable value. The waveform of the voltage measurement in the grounding resistance (V), in the field winding (V_f), and in the low-voltage side of the excitation transformer (V_{ph}) are analyzed to detect and locate the ground fault (see Fig. 1). In the measurement wave analyzer block, the harmonic components of the voltage measurements, necessary for the algorithm, are obtained [see Fig. 2(a)].

A. AC/DC-Side Discrimination

In case of ground fault in the excitation system, a current will flow through the grounding resistance, and the frequency of the grounding-resistance voltage (V) will depend on the position

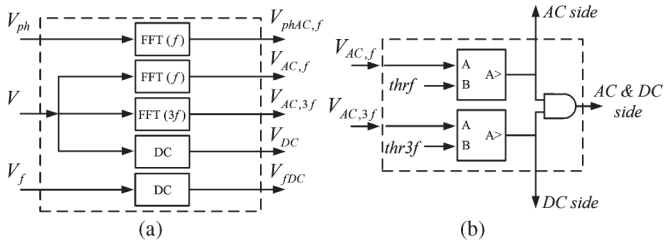

Fig. 2. Scheme of (a) the measurement wave analyzer block and (b) the ac–dc discrimination block.

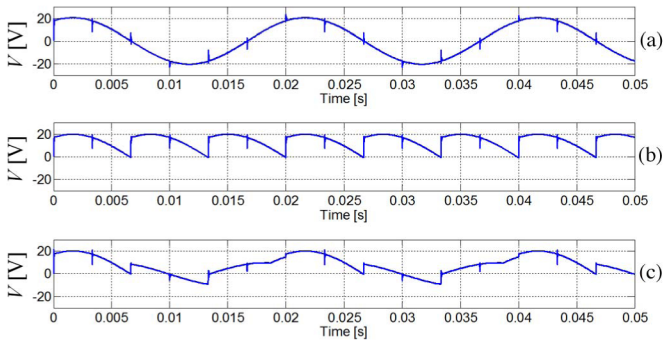

Fig. 3. Grounding-resistance voltage waveform for different fault points, namely, (a) ac side, (b) dc side, (c) simultaneous ac- and dc-side faults, in a 5-kVA laboratory synchronous generator ($V_{fDC} = 20$ V, $R_F = 0\ \Omega$).

of the defect in the excitation circuit, ac side, dc side, or both. The following faults may be identified.

1) AC-side fault: The grounding voltage amplitude depends on the fault resistance value. Moreover, it has the network frequency f_1 [see Fig. 3(a)]; this is an usual ground-fault detection technique in ac distribution system.
2) DC-side fault: The wave amplitude depends on the fault resistance value, and its frequency is three times the network frequency, i.e., $3 \cdot f_1$ [see Fig. 3(b)]; this frequency is caused by the ripple of the thyristor rectifier output voltage.
3) Simultaneous ac- and dc-side faults: The waveform has first- and third-order harmonic components [f_1 and $3 \cdot f_1$; see Fig. 3(c)].

In conclusion, by analyzing the frequency of the grounding-resistance voltage, it is possible to differentiate whether the fault is on the ac or the dc side. This way, the ac–dc discrimination algorithm is based on the comparison of the fundamental and third-harmonic component to their own setting thresholds, i.e., $thrf$ and $thr3f$ [see Fig. 2(b)].

B. Field Winding Ground-Fault Location Method

The ac/dc-side discrimination detection method is based on the analysis of the frequency of the ac component of the voltage at the grounding resistance. However, in case of fault in the field winding, a dc component also appears in the voltage measurement of the grounding resistance.

The principle behind the location method is the linear relationship between the dc voltage component in the grounding resistance (V_{DC}) and the position of the fault along the field

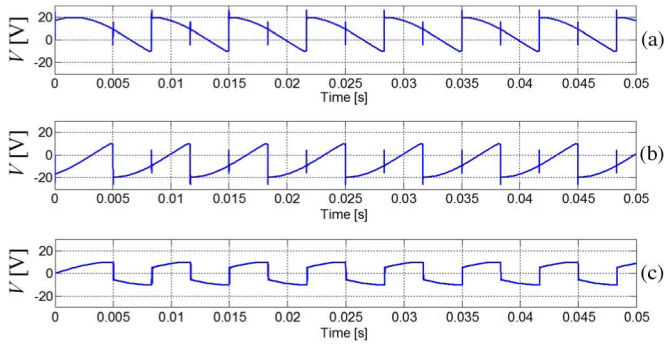

Fig. 4. Grounding-resistance voltage waveform for different fault points at the field winding, namely, (a) 0%, (b) 100%, and (c) 50%, in a 5-kVA laboratory synchronous generator ($V_{fDC} = 20$ V, $R_F = 0\ \Omega$).

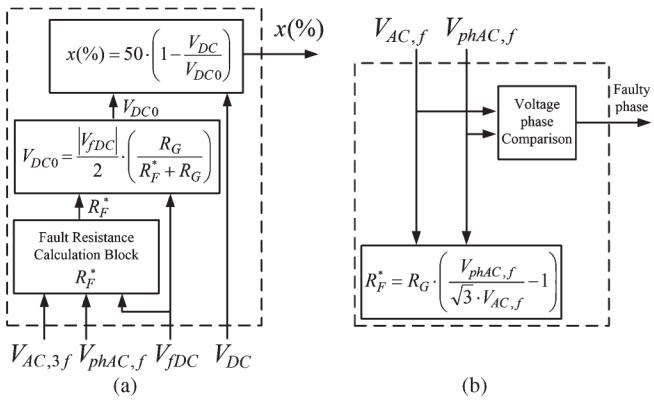

Fig. 5. Scheme of (a) the field winding ground-fault location block and (b) the ac-side detection block (see Fig. 1).

winding ($x(\%)$). The amplitude of V_{DC} has the maximum value, with positive polarity, when the fault occurs in the negative terminal, which is considered as the start of the winding ($x = 0\%$) (see Fig. 1), as shown in Fig. 4(a). On the other hand, if the fault occurs in the positive terminal, which is the end of the winding ($x = 100\%$), V_{DC} has the same amplitude, although the polarity is negative [see Fig. 4(b)]. However, V_{DC} is negligible for faults at the midpoint of the winding (50%), as shown in Fig. 4(c). In this laboratory case, the dc component of the excitation voltage V_{fDC} was adjusted to 20 V, and the grounding resistance R_G was set to 1 kΩ. According to [44], the maximum value of the dc component (V_{DC0}) depends on the value of the fault resistance R_F. Both parameters can be obtained through the following expressions:

$$V_{DC0} = \frac{|V_{fDC}|}{2} \cdot \left(\frac{R_G}{R_G + R_F}\right) \tag{1}$$

$$x(\%) = 50 \cdot \left(1 - \frac{V_{DC}}{V_{DC0}}\right). \tag{2}$$

Expression (1) shows the linear relationship between the dc component of the field voltage (V_{fDC}) and the maximum value of V_{DC}(V_{DC0}). This way, just measuring V_{DC}, the position of the ground fault ($x(\%)$) can be easily obtained using expression (2). The complete rotor fault location methodology

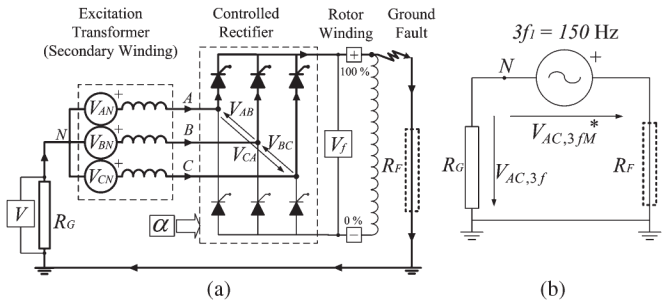

Fig. 6. (a) Simplified scheme of the excitation system in case of ground fault at 100% of the field winding. (b) Third-harmonic equivalent circuit.

is summarized in the scheme of the location block, as shown in Fig. 5(a).

C. AC-Side Ground-Fault Detection Algorithm

If the ground fault occurs on the ac side of the excitation system, the fault current depends both on the fault-resistance and the grounding-resistance value. In the worst-case scenario (the insulation failure is severe, and the fault resistance is close to zero), the fault current is limited only by the grounding resistance to a very low value, which allows the fault to be detected, but ensures no damage. The value of the fault resistance for every case of ac-side ground fault can be obtained by the following expression:

$$R_F^* = R_G \cdot \left(\frac{V_{phAC,f}}{\sqrt{3} \cdot V_{AC,f}} - 1 \right) \tag{3}$$

where $V_{phAC,f}$ is the ac component at f_1 of V_{ph}, and $V_{AC,f}$ is the ac component at f_1 of V. Moreover, the faulty phase is determined by phase comparison using $V_{phAC,f}$ and $V_{AC,f}$, since in case of ground fault at this part of the excitation system, the phase–neutral voltage of the faulty phase and the grounding-resistance voltage have the same phase angle. The algorithm for detecting ground faults on the ac side of the excitation system is summarized in Fig. 5(b).

III. Novel Estimation Method of Ground-Fault Resistance Value

When a solid ground fault occurs at any point of the field winding, a circulating current flows through the grounding resistor, and V is measured. For instance, in Fig. 6(a), a ground fault in the positive terminal (100%) of the field winding is represented, where α is the firing angle, V_{AB}, V_{BC}, V_{CA} are the phase-to-phase voltages, and V_{AN}, V_{BN}, V_{CN} are the phase–neutral voltages. As observed in this case, the ground fault is electrically connected to the terminal with the highest level of voltage (A, B, or C), which makes the waveform of V the same as the output of a three-phase half-wave rectifier, whereas V_f is not affected. In Fig. 7(a), the waveforms of V and V_f are represented for this case, considering the phase-to-phase voltage level $V_{phAC,f} = 314$ V and $\alpha = 60°$. As observed, the main frequency of V is 150 Hz ($3 \cdot f_1$), whereas the main frequency of V_f is 300 Hz ($6 \cdot f_1$). In the online location method previously presented [44], the fault resistance

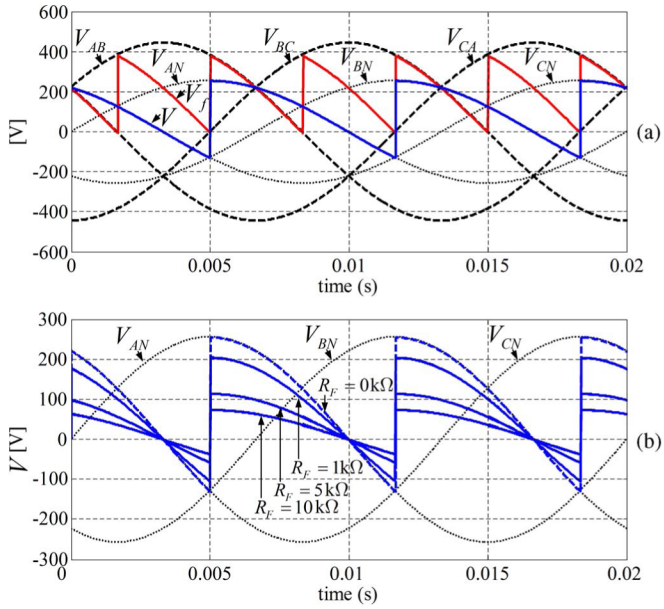

Fig. 7. (a) Waveforms of V, V_f, phase-to-phase voltages, and phase-to-ground voltages in case of ground fault at $x = 100\%$ of the field winding. (b) Influence of the fault resistance value on the grounding-resistance voltage, i.e., V.

value was obtained by the ratio between the $6 \cdot f_1$ component of $V_f (V_{fAC,6f})$ and the $3 \cdot f_1$ component of $V (V_{AC,3f})$, as expressed in the following equation:

$$R_F^* = R_G \cdot \left(\frac{V_{fAC,6f}}{V_{AC,3f}} - 1 \right). \tag{4}$$

Although the ratio between $V_{fAC,6f}$ and $V_{AC,3f}$ linearly varies, the accuracy of the calculation of R_F through this ratio may not be so accurate. For instance, in case of a solid ground fault ($R_F = 0\ \Omega$), while the value of this ratio should be 1, its actual value is 1.108. This fact leads to the necessity of calculating the value of R_F through a new algorithm described in this paper.

While the waveform of the voltage in the field winding (V_f) remains unalterable in case of ground fault of any R_F value and at any position, the waveform of the voltage in the grounding resistance (V) depends on the value of the fault resistance (R_F). The effect of the value of R_F in the measurement of V can be studied through the equivalent circuit in Fig. 6(b), where $V^*_{AC,3fM}$ is the maximum value of the $3 \cdot f_1$ component of the voltage measured in the grounding circuit, which corresponds to the case of $R_F = 0\ \Omega$. The $3 \cdot f_1$ component of $V (V_{AC,3f})$ is equal to $V^*_{AC,3fM}$ in case of $R_F = 0\ \Omega$; however, as the value of R_F is increased, the level of $V_{AC,3f}$ lowers. In Fig. 7(b), the waveform of V is represented in case of a ground fault at the positive terminal (100%) and $\alpha = 60°$, for several values of fault resistance.

Through the equivalent circuit represented in Fig. 6(b), the fault resistance value is calculated by the following expression:

$$R_F^* = R_G \cdot \left(\frac{V^*_{AC,3fM}}{V_{AC,3f}} - 1 \right). \tag{5}$$

Nonetheless, the value of $V^*_{AC,3fM}$ is only known in the case of $R_F = 0\ \Omega$. Therefore, the value of this variable has to be estimated, whereas the value of $V_{AC,3f}$ is obtained through fast Fourier transform analysis of the actual measurement of V.

For the estimation of $V^*_{AC,3fM}$, the value of the firing angle has to be obtained first. This variable (α^*) is calculated through the dc component of $V_f(V_{fDC})$ and the ac voltage supply $(V_{phAC,f})$, as observed in the following well-known expression:

$$\alpha^* = \arccos\left(\frac{V_{fDC}\cdot\pi}{3\cdot\sqrt{2}\cdot V_{phAC,f}}\right). \tag{6}$$

The waveform of V in case of a ground fault with $R_F = 0\ \Omega$ [see Fig. 7(b)] is the waveform of the output voltage of a half-wave rectifier, fed by the phase–neutral voltage of the secondary winding excitation transformer. This waveform is decomposed in Fourier components through the following expression:

$$V(t) = V_0 + \sum_{n=1}^{\infty}\left(A_n\cos(n\cdot\omega_0\cdot t) + B_n\sin(n\cdot\omega_0\cdot t)\right) \tag{7}$$

where ω_0 is the angular frequency, related to the fundamental frequency of the waveform $f_0(f_0 = 3\cdot f_1)$, and n is the harmonic order. For this voltage waveform, the fundamental frequency is $3\cdot f_1$ (150 Hz); hence, coefficients A_1 and B_1 correspond to the frequency components of 150 Hz. Hence, $V^*_{AC,3fM}$ (rms) is obtained by expression (8), which depends on α^* and $V_{phAC,f}$. Thus,

$$V^*_{AC,3fM} = \sqrt{\frac{1}{2}\cdot(A_1^2 + B_1^2)} = f(\alpha^*, V_{phAC,f}). \tag{8}$$

These coefficients are obtained through the following expressions:

$$A_1 = \frac{3}{\pi}\cdot\int_{\frac{\pi}{6}+\alpha}^{\frac{5\pi}{6}+\alpha}\sqrt{\frac{2}{3}}\cdot V_{phAC,f}\cdot\sin t\cos 3t\ dt \tag{9}$$

$$B_1 = \frac{3}{\pi}\cdot\int_{\frac{\pi}{6}+\alpha}^{\frac{5\pi}{6}+\alpha}\sqrt{\frac{2}{3}}\cdot V_{phAC,f}\cdot\sin t\sin 3t\ dt. \tag{10}$$

Finally, expressions (11) and (12) show the value of these components and its dependability on the firing angle, previously obtained, i.e.,

$$A_1 = \frac{3\sqrt{2}\cdot V_{phAC,f}\cdot\cos\alpha\sin\alpha\cdot(3-3\cdot\cos\alpha^2-\text{sen}\,\alpha^2)}{2\pi} \tag{11}$$

$$B_1 = -\frac{3\sqrt{2}\cdot V_{phAC,f}\cdot(2\cdot\cos 2\alpha-\cos 4\alpha)}{8\pi}. \tag{12}$$

Through A_1 and B_1, the value of $V^*_{AC,3fM}$ is obtained. Finally, the estimated value of the fault resistance (R^*_F) is calculated by expression (5), where $V^*_{AC,3fM}$ is obtained by the algorithm, and $V_{AC,3f}$ is obtained from the actual measurement of V. The simplified scheme of the fault-resistance calculation algorithm is summarized in Fig. 8. One of the advantages of obtaining R^*_F by comparing $V_{AC,3f}$ with $V^*_{AC,3fM}$ (5) is

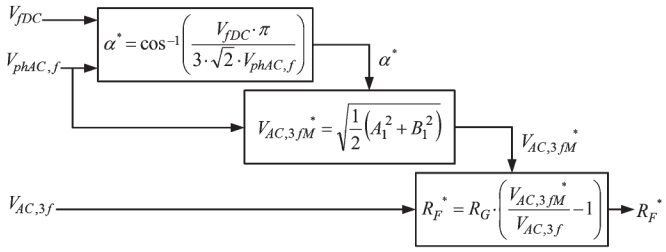

Fig. 8. Simplified scheme of the fault resistance calculation block R^*_F.

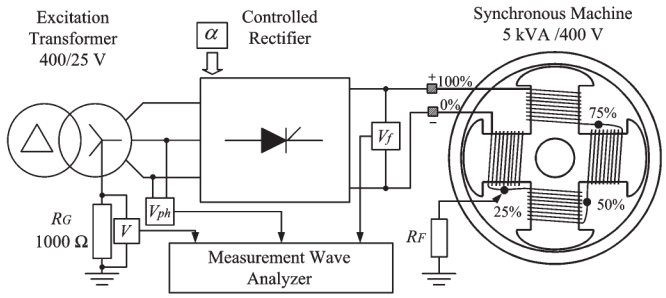

Fig. 9. Simplified block diagram of the experimental setup in the 5-kVA synchronous machine.

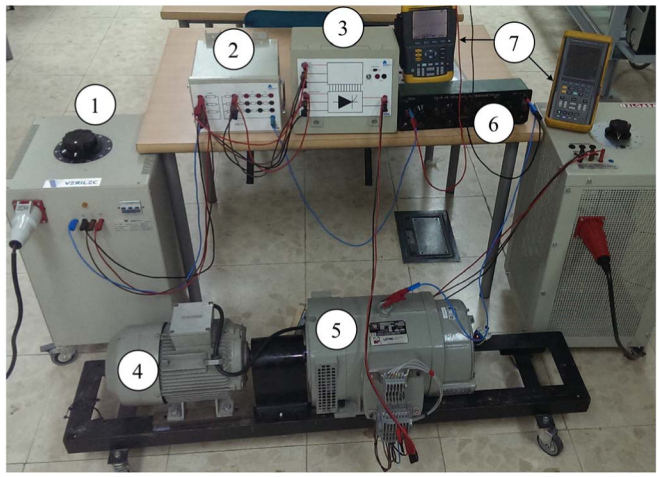

Fig. 10. Laboratory experimental setup: (1) power supply of the excitation transformer; (2) excitation transformer; (3) controlled rectifier; (4) asynchronous motor, prime mover; (5) 5-kVA synchronous generator; (6) grounding resistance; (7) oscilloscopes.

that, although the value of $V_{AC,3f}$ decreases as R_F increases, the value of $V^*_{AC,3fM}$ remains constant, because it depends exclusively on α^* and $V_{phAC,f}$ [see (8)], which makes the comparison very robust.

IV. Experimental Results in a 5-kVA Laboratory Synchronous Generator

Experimental tests have been performed in a real synchronous generator to evaluate the increase in accuracy in the fault location, by the integration of the fault-resistance estimation algorithm within the location method. The tests have been carried out in a laboratory setup, whose simplified scheme is shown in Fig. 9. The 5-kVA synchronous generator is specially designed to perform rotor ground faults, since some points of the rotor winding are accessible (25%, 50%, and 75%). In

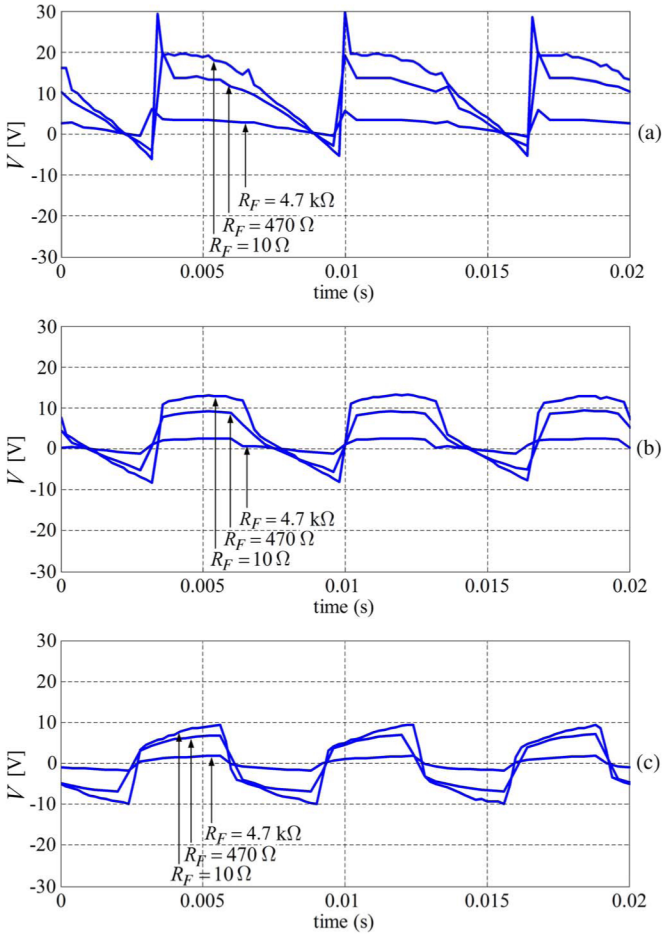

Fig. 11. Waveform of the voltage in the grounding resistance (V), for several values of fault resistance, in case of ground fault at (a) $x = 0\%$, (b) $x = 25\%$, and (c) $x = 50\%$, in a laboratory 5-kVA synchronous generator.

Fig. 10, a picture of the experimental setup is shown, where all the components can be identified.

For several values of ground-fault resistance, ground faults were performed in the accessible points of the rotor winding, as well as at the negative terminal (0%) and the positive terminal (100%). The results were registered by an oscilloscope and analyzed with MATLAB, where the algorithm was executed. In Fig. 11, the waveforms of the voltage in the grounding resistance, i.e., V, obtained during the ground-fault tests are represented. The ratio of the excitation transformer used in these tests is 400/25 V ($V_{phAC,f} = 25$ V). The excitation voltage (V_{fDC}) is 20 V, which implies a firing angle α of 54° approximately. As described, in case of ground fault in the negative terminal of the field winding (0%), the dc component of V has positive polarity [see Fig. 11(a)]. However, its magnitude depends on the fault resistance value. As the fault resistance value increases, the magnitude of V_{DC} lowers.

In Fig. 11(b) and (c), the waveforms of V are represented for ground fault at 25% and 50% of the field winding, respectively, for several values of fault resistance. As observed in both figures, the magnitude of V is yet again lower for higher values of fault resistance (4.7 kΩ).

In Tables I–III, the results of the location algorithm during ground-fault tests are summarized. For each value of fault resistance, the values of the variables needed to perform the location algorithm (V_{fDC}, V_{DC}, and $V_{AC,3f}$) are listed. The results of the variables obtained by the algorithm (α^*, $V^*_{AC,3fM}$, R^*_F, and the estimation of the fault location, x^*) are also summarized. As observed in Table I (ground fault in 25% of the field winding), while the magnitude of V_{DC} and $V_{AC,3f}$ is reduced when R_F increases, the magnitude of $V^*_{AC,3fM}$, obtained by the algorithm, remains constant. As expected, in Table II (ground fault in 50% of the field winding), it is observed that the magnitude of V_{DC} remains very close to zero for any value of fault resistance.

TABLE I
TEST RESULTS OF A GROUND FAULT IN 25% OF THE FIELD WINDING OF THE LABORATORY 5-kVA SYNCHRONOUS GENERATOR

R_F [Ω]	10	47	470	1000	4700
$V_{f,DC}[V]$	19.5	20	19.7	20	19.9
$V_{DC}[V]$	4.9	4.8	3.3	2.5	0.9
$V_{AC,3f}[V]$	6,9	6,5	4,9	3,3	1,23
$\alpha^*[deg]$	54.7	53.7	54.3	53.7	53.9
$V_{AC,3fM}{}^*[V]$	7.55	7.43	7.54	7.43	7.50
R^*_F [Ω]	94.8	142.5	539.8	1250.3	5094.6
$x^*(\%)$	24.08	24.07	25.81	23.22	23.92

TABLE II
TEST RESULTS OF A GROUND FAULT IN 50% OF THE FIELD WINDING OF THE LABORATORY 5-kVA SYNCHRONOUS GENERATOR

R_F [Ω]	10	47	470	1000	4700
$V_{f,DC}[V]$	19.8	19.8	20.1	20.5	19.8
$V_{DC}[V]$	0.1	-0.1	-0.1	0.1	0.1
$V_{AC,3f}[V]$	6.7	6.2	5.2	3.3	1.22
$\alpha^*[deg]$	54.1	54.0	53.3	52.6	54.1
$V_{AC,3fM}{}^*[V]$	7.50	7.50	7.48	7.41	7.50
R^*_F [Ω]	120.1	210.4	586.9	1244.8	5151.1
$x^*(\%)$	49.43	50.61	50.78	48.90	49.68

TABLE III
TEST RESULTS OF A GROUND FAULT IN 75% OF THE FIELD WINDING OF THE LABORATORY 5-kVA SYNCHRONOUS GENERATOR

R_F [Ω]	10	47	470	1000	4700
$V_{f,DC}[V]$	20	19.8	20.2	19.4	19.5
$V_{DC}[V]$	-4.9	-4.8	-3.3	-2.4	-0.9
$V_{AC,3f}[V]$	6.9	6.3	4.9	3.4	1.26
$\alpha^*[deg]$	53.	54.1	53.3	54.9	54.7
$V_{AC,3fM}{}^*[V]$	7.43	7.50	7.40	7.59	7.55
R^*_F [Ω]	76.3	191.2	586.9	1233.6	4995.1
$x^*(\%)$	74.53	76.98	74.86	75.76	74.29

As observed in these tables, the accuracy of the fault resistance obtained through the algorithm (R^*_F) is improved for higher values of fault resistance. In this laboratory-scale setup, the precision of the measurement of V_{ph} or the accuracy in the calculation of α^* and $V^*_{AC,3fM}$ implies large error in the calculation of R^*_F for lower values of fault resistance. Even so, the results of the ground-fault location (x^*) show satisfactory accuracy (less than 2% error) in every test. The improvement of the accuracy in the location algorithm is observed in Table IV, in which the results of the fault location and its error (x^* and E) is compared with the previous method (x^*_p and E_p).

V. EXPERIMENTAL RESULTS IN A 106-MVA COMMERCIAL SYNCHRONOUS GENERATOR

This novel location method was tested in a 12-kV 106-MVA hydro-synchronous generator, whose data are summarized in

TABLE IV
COMPARISON BETWEEN THE RESULTS OF THE APPLICATION OF THIS LOCATION METHOD AND THE METHOD PREVIOUSLY PRESENTED; LABORATORY 5-kVA SYNCHRONOUS GENERATOR

x (%)	R_F [Ω]	x^* (%)	E (%)	x_p^* (%)	E_p (%)
25	10	24.08	-0.92	26.34	1.34
25	470	25.81	0.81	26.87	1.87
25	4700	23.92	-1.08	26.32	1.32
50	10	49.43	-0.57	49.59	-0.41
50	470	50.78	0.78	49.32	-0.68
50	4700	49.68	-0.32	48.49	-1.51
75	10	74.53	-0.47	71.72	-3.28
75	470	74.86	-0.14	73.22	-1.78
75	4700	74.29	-0.71	72.55	-2.45

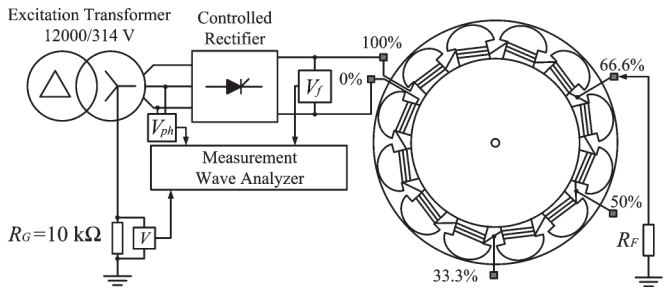

Fig. 12. Simplified block diagram of the experimental setup in the 106-MVA hydro generator.

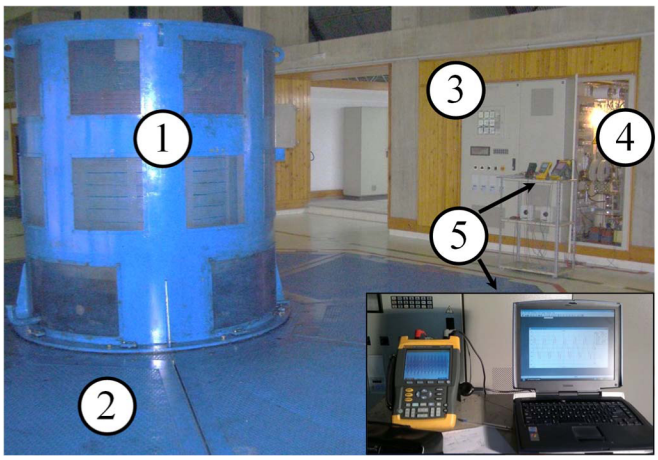

Fig. 13. Setup of the field test: (1) 5.5-MW asynchronous motor; (2) 106-MVA generator; (3) automatic voltage regulator (Unitrol F); (4) field breaker; (5) additional equipment for field measurements.

Table XI of the Appendix. The field winding is composed of 12 poles, and the excitation transformer is 12 kV/314 V, which implies $V_{phAC,f} = 314$ V.

Ground-fault tests were performed in some of the interpole connections (0%, 33.3%, 50%, 66.6%, and 100%) of the field winding, with several values of fault resistance and $R_G = 10$ kΩ (see Fig. 12). Voltages V, V_f, and V_{ph} were registered with an oscilloscope and postanalyzed with MATLAB, where the algorithm is executed. The experimental setup for the field test is shown in Fig. 13, where the main components of the scheme can be identified. The most significant waveforms of V, obtained during ground-fault tests, are represented in Fig. 14. As expected, the magnitude of V is reduced as the fault resistance value is increased in each case. Moreover, the symmetry

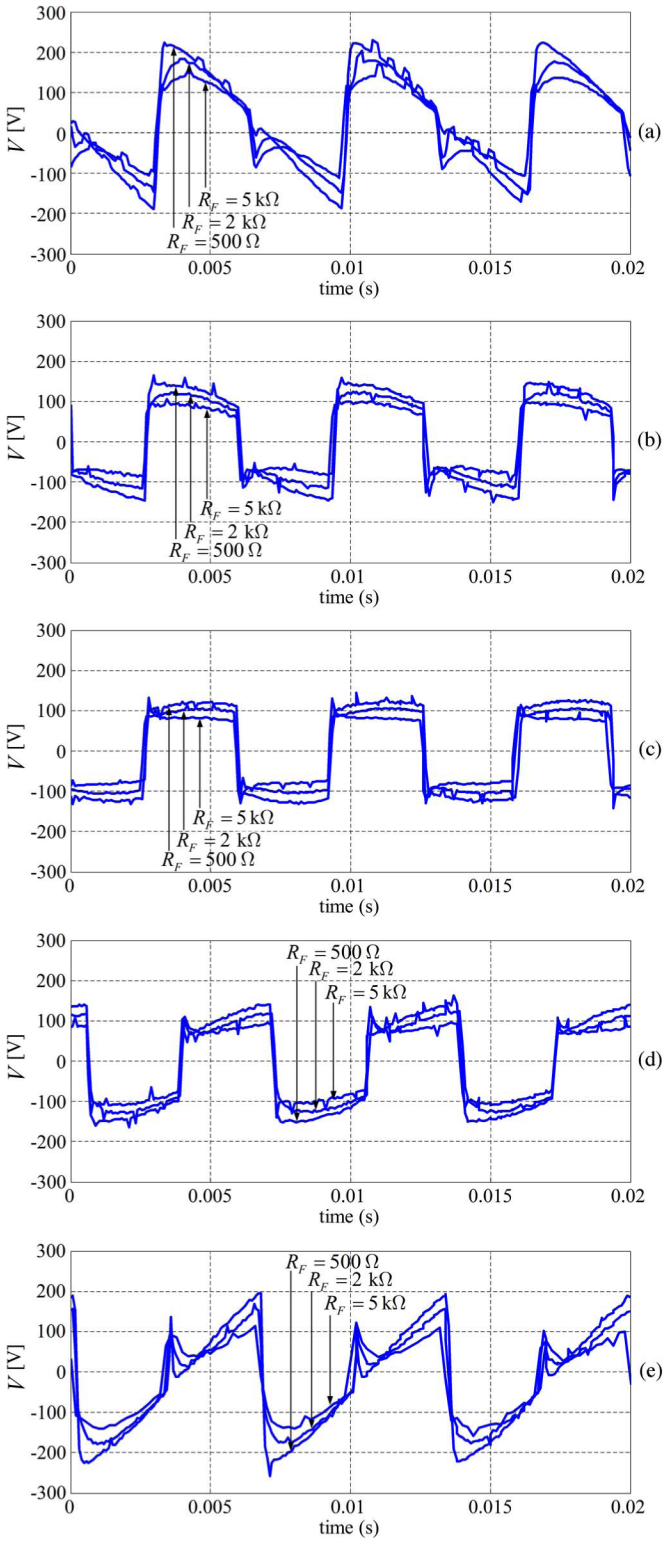

Fig. 14. Waveform of the voltage in the grounding resistance (V), for several values of fault resistance, in case of ground fault at (a) $x = 0\%$, (b) $x = 33.3\%$, (c) $x = 50\%$, (d) $x = 66.6\%$, and (e) $x = 100\%$, in a commercial 106-MVA synchronous generator.

of the waveform in case of fault in 33.3% and 66.6% and in 0% and 100% can be observed. In Tables V–IX, the quantitative results of the ground-fault tests are summarized. As observed in these tables, as the value of fault resistance increases, the

TABLE V
TEST RESULTS OF A GROUND FAULT IN 0% OF THE FIELD WINDING OF THE COMMERCIAL 106-MVA SYNCHRONOUS GENERATOR

R_F [Ω]	500	2000	5000	8000	10000
$V_{f,DC}[V]$	51.0	51.1	47.5	49.2	43.1
$V_{DC}[V]$	24.3	20.1	15.9	14.3	11.9
$V_{AC,3f}[V]$	108.2	92.0	80.4	72.0	71.1
$\alpha^*[deg]$	83.1	83.1	83.6	83.4	84.1
$V_{AC,3fM}{}^*[V]$	111.72	111.72	111.82	111.77	111.92
R_F^* [Ω]	344.2	2143.2	3977.5	5523.6	5763.4
$x^*(\%)$	0.71	2.21	2.80	4.85	6.38

TABLE VI
TEST RESULTS OF A GROUND FAULT IN 33.3% OF THE FIELD WINDING OF THE COMMERCIAL 106-MVA SYNCHRONOUS GENERATOR

R_F [Ω]	500	2000	5000	8000	10000
$V_{f,DC}[V]$	45.0	49.1	50.0	47.2	50.1
$V_{DC}[V]$	7.0	6.7	5.8	4.1	3.2
$V_{AC,3f}[V]$	107.2	90.1	72.2	68.0	66.1
$\alpha^*[deg]$	83.9	83.4	83.2	83.6	83.2
$V_{AC,3fM}{}^*[V]$	111.87	111.77	111.74	111.82	111.74
R_F^* [Ω]	455.1	2418.9	5519.4	6444.1	6930.3
$x^*(\%)$	33.74	33.02	32.00	36.00	39.84

TABLE VII
TEST RESULTS OF A GROUND FAULT IN 50% OF THE FIELD WINDING OF THE COMMERCIAL 106-MVA SYNCHRONOUS GENERATOR

R_F [Ω]	500	2000	5000	8000	10000
$V_{f,DC}[V]$	50.0	47.2	45.3	47.0	48.1
$V_{DC}[V]$	-0.6	-0.7	-0.9	0.9	-1.0
$V_{AC,3f}[V]$	107.1	90.0	74.2	67.0	66.1
$\alpha^*[deg]$	83.2	83.6	83.9	83.6	83.5
$V_{AC,3fM}{}^*[V]$	111.75	111.82	111.87	111.82	111.80
R_F^* [Ω]	443.9	2424.4	5117.6	6689.6	6939.4
$x^*(\%)$	51.25	51.85	53.02	46.63	53.53

TABLE VIII
TEST RESULTS OF A GROUND FAULT IN 66.6% OF THE FIELD WINDING OF THE COMMERCIAL 106-MVA SYNCHRONOUS GENERATOR

R_F [Ω]	500	2000	5000	8000	10000
$V_{f,DC}[V]$	50.2	46.0	49.1	46.0	51.3
$V_{DC}[V]$	-10.0	-8.2	-7.1	-6.3	-7.0
$V_{AC,3f}[V]$	110.1	94.1	80.0	73.3	71.2
$\alpha^*[deg]$	83.2	83.8	83.4	83.8	83.1
$V_{AC,3fM}{}^*[V]$	111.75	111.85	111.48	111.74	111.72
R_F^* [Ω]	158.8	1899.3	3935.6	5307.7	5734.9
$x^*(\%)$	70.32	70.69	69.91	69.97	71.60

TABLE IX
TEST RESULTS OF A GROUND FAULT IN 100% OF THE FIELD WINDING OF THE COMMERCIAL 106-MVA SYNCHRONOUS GENERATOR

R_F [Ω]	500	2000	5000	8000	10000
$V_{f,DC}[V]$	53.0	51.3	49.2	49.1	48.1
$V_{DC}[V]$	-26.1	-22.1	-18.3	-16.7	-15.8
$V_{AC,3f}[V]$	109.1	93.3	78.2	69.0	66.2
$\alpha^*[deg]$	82.8	83.1	83.4	83.4	83.5
$V_{AC,3fM}{}^*[V]$	111.62	111.71	111.77	111.77	111.80
R_F^* [Ω]	240.4	2012.7	4329.8	6198.4	6939.4
$x^*(\%)$	100.46	102.07	103.57	105.04	105.69

magnitude of V_{DC} and $V_{AC,3f}$ is reduced, whereas the obtained $V_{AC,3fM}^*$ remains constant. In case of defect in 50% (see Table VII) of the field winding, the magnitude of V_{DC} is again very close to zero, as expected. The accuracy of the calculation of the fault-resistance value leads to very good results of fault location for $R_F < 5$ kΩ, with location errors lower than 4%. These values of error are considerably interesting for the application to commercial synchronous generators. Concretely, in some hydro-synchronous generators, where every single pole can be individually extracted, this location algorithm can turn out to be highly interesting, since it may allow for the identification of the pole under fault. It would avoid the extraction of the whole rotor, which is a very expensive operation.

TABLE X
COMPARISON BETWEEN THE RESULTS OF THE APPLICATION OF THIS LOCATION METHOD AND THE METHOD PREVIOUSLY PRESENTED; COMMERCIAL 106-MVA SYNCHRONOUS MACHINE

x (%)	R_F [Ω]	x^* (%)	E (%)	x_p^* (%)	E_p (%)
0	500	0.71	0.71	1.27	1.27
0	2000	2.21	2.21	2.49	2.49
0	5000	2.80	2.80	3.22	3.22
33.3	500	33.74	0.44	32.34	-0.96
33.3	2000	33.02	-0.28	31.16	-2.14
33.3	5000	32.00	-1.30	30.67	-2.63
50	500	51.25	1.25	51.41	1.41
50	2000	51.85	1.85	52.04	2.04
50	5000	53.02	3.02	53.27	3.27
66.6	500	70.32	3.72	72.67	6.07
66.6	2000	70.69	4.09	74.79	8.19
66.6	5000	69.91	3.31	71.83	5.23
100	500	100.46	0.46	100.79	0.79
100	2000	102.07	2.07	102.33	2.33
100	5000	103.57	3.57	104.64	4.64

The results of the application of the complete location method in the commercial 106-MVA generator are summarized in Table X, where results obtained through the previous method (x_p^* and E_p) and through the algorithm presented in this paper (x^* and E) are compared. As observed, the incorporation of this new fault-resistance value estimation algorithm in the location method provides more accurate results, thus reducing the error in every case.

Finally, some comments have to be mentioned regarding the comparison between the results of the application of the location method to the laboratory 5-kVA synchronous machine (see Table IV) and to the commercial 106-MVA generator (see Table X). As can be observed, the results in the laboratory machine are considerably better than the results in the large generator. This is due to the effect of the capacitance-to-ground of the field winding. In the 5-kVA synchronous machine, the value of the capacitance-to-ground is very low, and its effect is completely undetectable. In commercial machines, such as the 106-MVA synchronous machine, where the algorithm has been tested, this parameter has a low effect for $R_F < 5$ kΩ. However, the effect of the capacitance-to-ground makes the error higher for $R_F > 5$ kΩ, as observed in Tables V–IX. This latter fact does not reduce the applicability of this new location method, taking into account that the conventional ground-fault protective systems provide an alarm, typically when the equivalent impedance is lower than 3–4 kΩ. The trip in these devices is commonly set to 1–2 kΩ, where the algorithm presents the best accuracy.

TABLE XI
CHARACTERISTICS OF SYNCHRONOUS MACHINE

Rated apparent power	106	MVA
Rated Power Factor	0.8	
Rated voltage ($\pm$ 5.0%)	12	kV
Frequency	50	Hz
Rated speed	500	rpm
Direct-axis synchronous reactance (unsat) X_d	1.05	pu
Quadrature-axis synchronous reactance X_q	0.70	pu
Direct-axis subtransient reactance (unsat) X'_d	0.26	pu
Direct-axis subtransient reactance (unsat) X''_d	0.19	pu
Quadrature-axis subtransient reactance X''_q	0.19	pu
Direct-axis transient open-circuit time constant T'_{do}	9.5	s
Direct-axis transient short-circuit time constant T'_d	1.6	s
Direct-axis subtransient short-circuit time constant T''_d	32	ms
Rated field current I_{fN}	1060	A
Rated field voltage U_{fN}	241	V
Excitation transformer		
Winding connection	Dyn5	
Primary winding voltage	12	kV
Secondary winding voltage	0.314	kV
Rated power	630	kVA
Thyristor bridge		
Maximum output voltage	397	V
Minimum firing angle	15°	

VI. CONCLUSION

In this paper, a new algorithm for the calculation of the rotor ground-fault resistance value in synchronous machines with static excitation has been presented. This new algorithm is an improvement of an online ground-fault location method previously presented, whose application requests the installation of a grounding resistance in the secondary winding of the excitation transformer.

In the previously presented method, the fault resistance value was calculated through the ratio between the sixth-harmonic component of the field voltage and the third-harmonic component of the voltage in the grounding resistance, which introduced an error in the fault location. The new algorithm presented in this work is based on the comparison between the third-harmonic component of the voltage in the grounding resistance and the third-harmonic voltage calculated through the algorithm. This latter voltage is obtained through the measurements of the dc output voltage of the controlled rectifier and the ac supply voltage of this converter.

This new algorithm for calculating the fault-resistance value has the following major advantages: First, it does not need extra measurements or equipment, since the calculation is obtained with the field-winding voltage and the voltage measurement at the grounding resistance. Second, it may be easily implemented in modern protective relays. Finally, it can provide an accurate value of fault resistance in an online operating condition, which allows the location method to give a more precise location of faults that only occur while rotating.

The improvement of the accuracy in the calculation of the fault resistance value allows for improving the accuracy of the online ground-fault location method. The complete location method has been first tested in a 5-kVA laboratory synchronous generator, with satisfactory results, thus reducing the location error more than three times in some cases, obtaining errors below 1% in most of the tests. Second, this location method has also been tested in a 106-MVA hydro-synchronous generator. The positive results of these tests show a reduction in the location error of more than 4% in some cases.

The results presented in this work increase the interest in the ground-fault location in an online operating condition. The application of this new fault-resistance estimation algorithm and the online location method in commercial synchronous generators may become interesting for the industry. It may help drastically reduce repair time and cost, after the detection of a ground fault, as it can be accurately located. Concretely, in some hydro-synchronous generators, where every single pole can be individually extracted, this location method can turn out to be highly interesting, since it may avoid the extraction of the whole rotor, which is a very expensive operation.

APPENDIX

See Table XI.

ACKNOWLEDGMENT

The authors would like to thank the E.on staff for the technical support.

REFERENCES

[1] *IEEE Guide for AC Generator Protection*, IEEE Std C37.102-2006 (Revison of IEEE Std C37.102-1995), Aug. 21, 2013, pp. 1–173.
[2] R. J. Zawosky and W. M. Genoverse, "Generator thermal sensitivity, theory and experience," GE Power Systems, Schenectady, NY, USA, GER-3809, Apr. 2001.
[3] A. Tetreault, "Rotor shape vs. rotor field pole shorted turns: Impact on rotor induced vibrations on hydrogenerators," in *Proc. CMD*, Sep. 23–27, 2012, pp. 133–136.
[4] R. J. Zawosky and K. C. Tornroos, "GE generator rotor design, operational issues and refurbishment options," GE Power Systems, Schenectady, NY, USA, GER-3809, Aug. 2001.
[5] C. V. Maughan and J. M. Reschovsky, "Advances in motor and generator rotor health," in *Proc. IEEE ISEI*, Jun. 6–9, 2010, pp. 1–4.
[6] M. Kiani, W.-J. Lee, R. Kenarangui, and B. Fahimi, "Detection of rotor faults in synchronous generators," in *Proc. IEEE SDEMPED*, Sep. 6–8, 2007, pp. 266–271.
[7] M. L. Miller, "General concepts related to turbine generator insulation materials used in rotor windings," in *Proc. IEEE EIC*, May 31–Jun. 3, 2009, pp. 328–332.
[8] E. A. Boulter and G. C. Stone, "Historical development of rotor and stator winding insulation materials and systems," *IEEE Electr. Insul. Mag.*, vol. 20, no. 3, pp. 25–39, May/Jun. 2004.
[9] G. C. Stone, "Recent important changes in IEEE motor and generator winding insulation diagnostic testing standards," *IEEE Trans. Ind. Appl.*, vol. 41, no. 1, pp. 91–100, Jan./Feb. 2005.
[10] M. Kiani, W.-J. Lee, R. Kenarangui, and B. Fahimi, "Frequency domain methods for detection of rotor faults in synchronous machines under no-load condition," in *Proc. 39th NAPS*, Sep. 30–Oct. 2, 2007, pp. 31–36.
[11] R. L. Stoll and A. Hennache, "Method of detecting and modelling presence of shorted turns in DC field winding of cylindrical rotor synchronous machines using two airgap search coils," *Proc. Inst. Elect. Eng.—Elect. Power Appl.*, vol. 135, no. 6, pp. 281–294, Nov. 1988.
[12] C. A. P. Gaona, F. Blázquez, P. Frías, and M. Redondo, "A novel rotor ground-fault-detection technique for synchronous machines with static excitation," *IEEE Trans. Energy Convers.*, vol. 25, no. 4, pp. 965–973, Dec. 2010.
[13] I. Kerszenbaum and J. Lopetrone, "Novel Hall-effect turbo-generator's rotor DC ground-fault localizer," in *Proc. IEEE Int. Elect. Mach. Drives Conf. Rec.*, May 18–21, 1997, pp. TC1/5.1–TC1/5.3.
[14] A. Bellini, F. Filippetti, C. Tassoni, and G.-A. Capolino, "Advances in diagnostic techniques for induction machines," *IEEE Trans. Ind. Electron.*, vol. 55, no. 12, pp. 4109–4126, Dec. 2008.
[15] A. Bellini, A. Yazidi, F. Filippetti, C. Rossi, and G.-A. Capolino, "High frequency resolution techniques for rotor fault detection of induction machines," *IEEE Trans. Ind. Electron.*, vol. 55, no. 12, pp. 4200–4209, Dec. 2008.

[16] F. Filippetti, A. Bellini, and G. Capolino, "Condition monitoring and diagnosis of rotor faults in induction machines: State of art and future perspectives," in *Proc. IEEE WEMDCD*, Mar. 11/12, 2013, pp. 196–209.
[17] Y. Gritli *et al.*, "Advanced diagnosis of electrical faults in wound-rotor induction machines," *IEEE Trans. Ind. Electron.*, vol. 60, no. 9, pp. 4012–4024, Sep. 2013.
[18] A. Stefani *et al.*, "Doubly fed induction machines diagnosis based on signature analysis of rotor modulating signals," *IEEE Trans. Ind. Appl.*, vol. 44, no. 6, pp. 1711–1721, Nov./Dec. 2008.
[19] A. Stefani, A. Bellini, and F. Filippetti, "Diagnosis of induction machines' rotor faults in time-varying conditions," *IEEE Trans. Ind. Electron.*, vol. 56, no. 11, pp. 4548–4556, Nov. 2009.
[20] C. Concari, G. Franceschini, C. Tassoni, and A. Toscani, "Validation of a faulted rotor induction machine model with an insightful geometrical interpretation of physical quantities," *IEEE Trans. Ind. Electron.*, vol. 60, no. 9, pp. 4074–4083, Sep. 2013.
[21] J. Seshadrinath, B. Singh, and B. K. Panigrahi, "Vibration analysis based interturn fault diagnosis in induction machines," *IEEE Trans. Ind. Informat.*, vol. 10, no. 1, pp. 340–350, Feb. 2014.
[22] L. Zarri *et al.*, "Detection and localization of stator resistance dissymmetry based on multiple reference frame controllers in multiphase induction motor drives," *IEEE Trans. Ind. Electron.*, vol. 60, no. 8, pp. 3506–3518, Aug. 2013.
[23] A. Yazidi, H. Henao, G.-A. Capolino, F. Betin, and L. Capocchi, "Experimental inter-turn short circuit fault characterization of wound rotor induction machines," in *Proc. IEEE ISIE*, Jul. 4–7, 2010, pp. 2615–2620.
[24] A. Yazidi, H. Henao, G.-A. Capolino, F. Betin, and L. Capocchi, "Inter-turn short circuit fault detection of wound rotor induction machines using Bispectral analysis," in *Proc. IEEE ECCE*, Sep. 12–16, 2010, pp. 1760–1765.
[25] A. Yazidi, H. Henao, G.-A. Capolino, and F. Betin, "Rotor inter-turn short circuit fault detection in wound rotor induction machines," in *Proc. ICEM*, Sep. 6–8, 2010, pp. 1–6.
[26] S. Toma, L. Capocchi, and G.-A. Capolino, "Wound-rotor induction generator inter-turn short-circuits diagnosis using a new digital neural network," *IEEE Trans. Ind. Electron.*, vol. 60, no. 9, pp. 4043–4052, Sep. 2013.
[27] Y.-H. Kim, Y.-W. Youn, D.-H. Hwang, J.-H. Sun, and D.-S. Kang, "High-resolution parameter estimation method to identify broken rotor bar faults in induction motors," *IEEE Trans. Ind. Electron.*, vol. 60, no. 9, pp. 4103–4117, Sep. 2013.
[28] K. N. Gyftakis and J. C. Kappatou, "Evaluation of the broken bar fault detectability depending on the rotor bar number," in *Proc. IEEE IECON*, Nov. 10–13, 2013, pp. 2798–2803.
[29] L. Saidi, H. Henao, F. Fnaiech, G.-A. Capolino, and G. Cirrincione, "Application of higher order spectral analysis for rotor broken bar detection in induction machines," in *Proc. IEEE SDEMPED*, Sep. 5–8, 2011, pp. 31–38.
[30] K. Bacha, M. Gossa, H. Henao, and G.-A. Capolino, "Comparative investigation of diagnosis media of stator voltage asymmetry and rotor broken bars in induction machines," in *Proc. IEEE IECON*, Nov. 6–10, 2006, pp. 5040–5045.
[31] S. D. Ochoa and M. Pacas, "Detection of rotor asymmetries in induction motors at standstill," in *Proc. IEEE ISIE*, May 28–31, 2013, pp. 1–6.
[32] F. Vedreno-Santos, M. Riera-Guasp, H. Henao, M. Pineda-Sanchez, and R. Puche-Panadero, "Diagnosis of rotor and stator asymmetries in wound-rotor induction machines under nonstationary operation through the instantaneous frequency," *IEEE Trans. Ind. Electron.*, vol. 61, no. 9, pp. 4947–4959, Sep. 2014.
[33] J. Antonino-Daviu, V. Climente-Alarcon, I. Tsoumas, G. Georgoulas, and R. B. Perez, "Multi-harmonic tracking for diagnosis of rotor asymmetries in wound rotor induction motors," in *Proc. IEEE IECON*, Nov. 10–13, 2013, pp. 5555–5560.
[34] A. Kontarcek, P. Bajec, M. Nemec, and V. Ambrozic, "Single open-phase fault detection in permanent magnet synchronous machine through current prediction," in *Proc. IEEE IECON*, Nov. 10–13, 2013, pp. 5860–5865.
[35] G. H. B. Foo, Z. Xinan, and D. M. Vilathgamuwa, "A sensor fault detection and isolation method in interior permanent-magnet synchronous motor drives based on an extended Kalman filter," *IEEE Trans. Ind. Electron.*, vol. 60, no. 8, pp. 3485–3495, Aug. 2013.
[36] A. Sarikhani and O. A. Mohammed, "Inter-turn fault detection in PM synchronous machines by physics-based back electromotive force estimation," *IEEE Trans. Ind. Electron.*, vol. 60, no. 8, pp. 3472–3484, Aug. 2013.
[37] C. Bruzzese, "Diagnosis of eccentric rotor in synchronous machines by analysis of split-phase currents—Part I: Theoretical analysis," *IEEE Trans. Ind. Electron.*, vol. 61, no. 8, pp. 4193–4205, Aug. 2014.
[38] C. Bruzzese, "Diagnosis of eccentric rotor in synchronous machines by analysis of split-phase currents—Part II: Experimental analysis," *IEEE Trans. Ind. Electron.*, vol. 61, no. 8, pp. 4206–4216, Aug. 2014.
[39] M. Biet, "Rotor faults diagnosis using feature selection and nearest neighbors rule: Application to a turbogenerator," *IEEE Trans. Ind. Electron.*, vol. 60, no. 9, pp. 4063–4073, Sep. 2013.
[40] G. C. Stone, M. Sasic, J. Stein, and C. Stinson, "Using magnetic flux monitoring to detect synchronous machine rotor winding shorts," in *Proc. IEEE PCIC*, Sep. 19–21, 2011, pp. 1–7.
[41] S. R. Campbell, J. Kapler, M. Sasic, and G. C. Stone, "Detection of rotor winding shorted turns in turbine generators and hydrogenerators," in *Proc. CIGRE*, 2010, pp. 1–12.
[42] A. Bacchus, M. Biet, L. Macaire, Y. Le Menach, and A. Tounzi, "Comparison of supervised classification algorithms combined with feature extraction and selection: Application to a turbo-generator rotor fault detection," in *Proc. IEEE SDEMPED*, Aug. 27–30, 2013, pp. 558–565.
[43] *IEEE Guide for Diagnostic Field Testing of Electric Power Apparatus—Electrical Machinery*, IEEE Std 62.2-2004, 2005, pp. 0_1–100.
[44] C. A. Platero, F. Blázquez, P. Frías, and M. Pardo, "New on-line rotor ground fault location method for synchronous machines with static excitation," *IEEE Trans. Energy Convers.*, vol. 26, no. 2, pp. 572–580, Jun. 2011.

Francisco R. Blánquez (S'12) was born in Spain in 1986. He received the Dipl. degree in electrical engineering from the Universidad Politécnica de Madrid, Madrid, Spain, in 2010, where he is currently working toward the Ph.D. degree in the Electrical Engineering Department.

His research interests include protective relaying for power systems, electrical machine diagnosis, and energy efficiency.

María Aranda was born in Spain in 1989. She received the Dipl. degree in electrical engineering from the Universidad Politécnica de Madrid, Madrid, Spain, in 2013.

Her research interests include protective relaying for power systems.

Emilio Rebollo (S'12) was born in Spain in 1986. He received the Dipl. degree in electrical engineering from the Universidad Politécnica de Madrid, Madrid, Spain, in 2010, where he is currently working toward the Ph.D. degree in the Electrical Engineering Department.

His research interests include electrical machine design and regulation of power plants.

Francisco Blázquez (M'07) was born in Toledo, Spain, on April 9, 1972. He received the Dipl. degree in industrial engineering and the Ph.D. degree in electrical engineering from the Universidad Politécnica de Madrid, Madrid, Spain, in 1997 and 2004, respectively.

Since 1999, he has been a Professor with the Electrical Engineering Department, Universidad Politécnica de Madrid. His current research interests include electrical machine design and wind power generation.

Carlos A. Platero (M'10) was born in Madrid, Spain, in 1972. He received the Dipl. degree and the Ph.D. degree in electrical engineering from the Universidad Politécnica de Madrid, Madrid, in 1996 and 2007, respectively.

From 1996 to 2008, he was with ABB Generación S.A., Alstom Power S.A., and ENDESA Generación S.A., where he was involved in design and commissioning of power plants. In 2002, he began teaching in the Electrical Engineering Department of the Universidad Politécnica de Madrid and joined an energy research group. Since 2008, he has been a full-time Associate Professor.